Renewable Energy 62 (2014) 556–562

Contents lists available at ScienceDirect

Renewable Energy

journal homepage: www.elsevier.com/locate/renene

Carbon supported Ag nanoparticles with different particle size as cathode catalysts for anion exchange membrane direct glycerol fuel cells

Zhichao Wang [a], Le Xin [a], Xusheng Zhao [a], Yang Qiu [a], Zhiyong Zhang [a], Olga A. Baturina [b], Wenzhen Li [a,*]

[a] Department of Chemical Engineering, Michigan Technological University, Houghton, MI 49931, USA
[b] Naval Research Lab, Washington, DC 20375, USA

ARTICLE INFO

Article history:
Received 1 March 2013
Accepted 12 August 2013
Available online 11 September 2013

Keywords:
Renewable energy
Non-precious metal
Nanoparticle
Electrocatalyst
Anion exchange membrane
Biorenewables

ABSTRACT

The effect of Ag particle size on oxygen reduction reaction (ORR) at the cathode was investigated in anion exchange membrane direct glycerol fuel cells (AEM-DGFC) with oxygen as an oxidant. At the anode, high purity glycerol (99.8 wt%) or crude glycerol (88 wt%, from soybean biodiesel) was used as fuel, and commercial Pt/C served as the anode catalyst. A solution phase-based nanocapsule synthesis method was successfully developed to prepare the non-precious Ag/C cathode catalyst, with $LiBEt_3H$ as a reducing agent. XRD and TEM characterizations show that as-synthesized Ag nanoparticles (NP) with a size of 2–9 nm are well dispersed on the Vulcan XC-72 carbon black support. Commercial Ag nanoparticles with a size of 20–40 nm were also supported on carbon black as a control sample. The results show that higher peak power density was obtained in AEM-DGFC employing an Ag-NP catalyst with smaller particle size: nanocapsule made Ag-NP > commercial Ag-NP (Alfa Aesar, 99.9%). With the nanocapsule Ag-NP cathode catalyst, the peak power density and open circuit voltage (OCV) of AEM-DGFC with high-purity glycerol at 80 °C are 86 mW cm^{-2} and 0.73 V, respectively. These are much higher than 45 mW cm^{-2} and 0.68 V for the AEM-DGFC with the commercial Ag/C cathode catalyst, which can be attributed to the enhanced kinetics and reduced internal resistance. Directly fed with crude glycerol, the AEM-DGFC with the nanocapsule Ag-NP cathode catalyst shows an encouraging peak power density of 66 mW cm^{-2}, which shows great potential of direct use of biodiesel waste fuel for electricity generation.

1. Introduction

The liquid alkaline fuel cells (AFCs) were one of the earliest fuel cell models that were developed in the beginning of the 1960s [1]. Because of the high output, current density and low cost of AFCs, extensive studies had been made during the 1960s to 1980s [2]. Although their popularity had been challenged by other types of fuel cells in recent years, particularly proton-exchange membrane fuel cells (PEMFCs), the resurgence of AFCs started with recent technology advances in solid anion exchange membranes (AEMs). The introduction of AEMs has brought several significant advantages over traditional AFCs and other acidic fuel cells, such as enhanced catalyst stability with negligible electro-kinetic performance losses, reduced corrosion problems associated with acid electrolyte, toleration of cheaper metal current collectors, no precipitated carbonate caused by mobile cations, reduced alcohol fuel crossover and the improvement in elimination of electrolyte leakage [2–5].

In an alkaline media, the electrocatalyst activity is higher than that in the acid media due to enhanced ion transport and facile charge transfer [6,7]. In addition, the poisoning effects on catalysts are also weak, and a wider range of metals are stable in an alkaline environment; thus, non-Platinum group metals can be used as electrocatalysts [6,7]. Ag has been found a promising cathode catalyst for a long time, because Ag shows high oxygen reduction reaction (ORR) activity at high pH, and a relatively high stability in a wide range of temperatures [8]. Furthermore, in an alkaline environment, the ORR activity on Ag is close to that on Pt [9,10]; however, the price of Ag is 100 times lower than precious metals, such as Pt and Pd. These merits make Ag a very attractive cathode catalyst. Ag-based electrocatalysts have attracted enormous research interest as an alternative to Pt for ORR in alkaline media [7,11–13]. Blizanac and co-workers have demonstrated that on Ag (111) single crystal, the ORR proceeds via a 4-electron-transfer pathway in high pH

* Corresponding author. Tel.: +1 906 487 2298; fax: +1 906 487 3213.
E-mail addresses: wzli@mtu.edu, liwenzhen@gmail.com (W. Li).

0960-1481/$ – see front matter © 2013 Elsevier Ltd. All rights reserved.
http://dx.doi.org/10.1016/j.renene.2013.08.005

media, with very little production of undesirable H_2O_2 by-product. It is also suggested that though Ag–$O_{(ads)}$ interaction is weaker when compared to Pt, it is still strong enough to facilitate dissociation of the O–O bond in a strong alkaline electrolyte [14]. The effect of carbon support on the pathway of ORR was also investigated in high pH media [15]. A 4-electron pathway was confirmed with regard to carbon supported Ag electro-catalysts in the base electrolyte [16]. Ag nanowire catalysts were also synthesized and 4-electron-transfer ORR was found to be predominant [8]. Chatenet et al. compared the ORR activity on Ag with that on Pt, and showed that in dilute base electrolyte, Ag was less active than Pt; however, with the base electrolyte concentration increasing, the ORR activities on Ag and Pt were comparable, and the 4-electron-transfer ORR pathway was confirmed on both catalysts [10].

Although significant amount of work has been done on investigation of ORR kinetics on Ag showing that Ag could be a good cathode catalyst candidate, those experiments were still based on half-cell tests. In the real fuel cell operation, other factors such as mass transport and diffusion, contact/ohmic resistance loss, and membrane electrode assembly (MEA) structure will also affect the overall fuel cell performance. There is a need to investigate the Ag catalyst behavior in the real fuel cell test. The research of Ag as a cathode catalyst in H_2–O_2 AEMFC had been reported by Varcoe et al. [17]. The maximum power density (*ca.* 50 mW cm^{-2} at 50 °C) was obtained with 4.0 mg cm^{-2} Ag/C (60 wt%) at the cathode. A similar work was conducted by Park et al. [18]. The loading of 2.0 mg cm^{-2} Ag/C (40 wt%) was used in their work and the peak power density of 30 mW cm^{-2} was achieved. Recently, Maheswari et al. [19] reported results on carbon-supported Ag (with different loading) cathode catalyst for H_2–O_2 AEMFC. Their results showed that the optimized fuel cell performance was achieved at 60 wt% Ag/C (metal loading) with a loading of 0.5 mg cm^{-2} catalyst. Through optimizing their test conditions, the highest peak power density can reach 10 mW cm^{-2}. Obviously, reducing Ag metal loading and increasing output power density are still in high demand.

It is well known that hydrogen is merely an energy carrier, but not a natural resource. The production, storage and transportation of hydrogen have encountered great challenges. Exploring renewable, reliable, and low-cost energy sources are an urgent need for global sustainable development. Fuel cells with different liquid fuels were developed very fast in the recent years. Compared to hydrogen-fed fuel cells, direct alcohol fuel cells (DAFCs) are more attractive due to the easy storage and purification of fuel, increased energy density, and environment friendliness [20–22]. Glycerol, one of the main byproducts from biodiesel production, can be obtained in large quantities at low price. Glycerol is also a non-toxic, non-volatile, and non-flammable fuel in contrast to the conventional methanol and ethanol fuels [23]. In addition, the energy density of glycerol (6.4 kWh L^{-1}) is comparatively higher than some small alcohols, such as methanol (4.8 kWh L^{-1}) [5]; thus, it is a promising fuel for biofuel cells or DAFCs. Matsuoka et al. [5] and Bambagioni et al. [24] investigated different types of anode catalysts, such as Pt–Ru/C and Pd/multi-walls carbon nanotube, as well as various cathode catalysts such as Ag/C and commercial Fe–Co based catalyst. In their glycerol/O_2 fueled fuel cell test, the peak power density is around 8 mW cm^{-2}. Later, better performances (in terms of power density) have been reported. For example, Matsuoka et al. investigated DAFCs fed with various alcohols. PtRu/C (4 mg cm^{-2}) and Pt/C (1 mg cm^{-2}) were used as anode and cathode catalysts, respectively. For the glycerol fuel, the peak power density of 27 mW cm^{-2} was achieved at 45 °C. A glycerol/O_2 enzymatic biofuel cell research has also been tested by Arechederra et al. Their biofuel cell has yielded a maximum power density of 1.21 mW cm^{-2} at room temperature [25]. Although enzymatic biofuel cell can completely oxidize glycerol to CO_2, their very low performance limits their applications to environmental remediation areas. There is still room for improvement for glycerol/O_2 fuel cell techniques by increasing the performance, reducing the amount of precious metal in the electrodes, and operating fuel cells directly fed with crude glycerol fuel.

In this article, we focused on the investigation of glycerol/O_2 AEM-DGFC using Ag/C cathode catalyst with two different particle sizes. Separated anode and cathode polarization curves were collected for the study of glycerol oxidation at the anode and oxygen reduction at the cathode. Electrochemical impedance spectroscopy was also used to analyze the reaction kinetics and internal resistance. Both high-purity glycerol (99.8 wt%) and industrial grade crude glycerol (88 wt%) were used as fuel, and considerable output power density was achieved using the crude glycerol under the test conditions.

2. Experimental

2.1. Synthesis of Ag/C catalysts with different particle size

The smaller size Ag/C catalyst with a metal loading of *ca.* 40 wt% was synthesized through a modified solution phase-based nanocapsule method [23,26–28]. Briefly, 83.5 mg silver acetate (0.5 mmol, Acros Organics, 99%) and 81.0 mg Vulcan XC-72R carbon black (Cabot) were mixed in 10 ml oleylamine (Aldrich Chemistry, 70%) with vigorous stirring in an inert nitrogen atmosphere. The temperature was kept at 30 °C while 0.7 ml $LiBEt_3H$ (1.0 M THF solution, Acros Organics) was injected into the solution. After kept the temperature for an additional 30 min, the final product (named as Ag/C-nanocapsule) was collected by filtration, washed with 800 ml ethanol, and dried overnight in a vacuum oven. For comparison, larger size Ag/C sample was obtained by impregnation method. In detail, 105 mg Vulcan XC-72R carbon black (Cabot) was dispersed in ethanol by sonication, and then, the carbon black was impregnated overnight with 70 mg of commercial Ag particles (Alfa Aesar, 99.9%) dispersed in hexane. After filtration, washing and overnight vacuum drying, the product marked as Ag/C-commercial was obtained.

2.2. Analysis of catalyst structures

The morphology, structure, and metal loading of Ag/C catalysts were analyzed by X-ray diffraction (XRD, Scintag XDS-2000, Cu K_α radiation, $\lambda = 1.5406$ Å, tube current of 35 mA, tube voltage of 45 kV, 2θ angles between 15° and 90°), transmission electron microscopy (TEM, JEOL 2010, operation voltage of 200 kV) and inductively coupled plasma atomic emission spectroscopy (ICP-AES).

2.3. Membrane electrode assembly (MEA) fabrication and single fuel cell test

The MEAs were fabricated with a commercial Pt/C-based anode and a self-made Ag/C-based cathode. The cathode catalyst ink was prepared by mixing Ag/C catalyst and AS-4 anion conductive ionomer (30 wt%, AS-4, Tokuyama) with 1-propanol as solvent. The mass ratio of Ag/C and AS-4 was 7:3. Similarly, the anode catalyst ink was prepared as follows: commercial Pt/C powder dispersed in iso-propanol containing 10 wt% polytetrafluoroethylene (PTFE), was used as hydrophobic agent that gave a good mechanical stability of the active layer and also prevented the electrode from being flooded by the electrolyte during operation [29]. The mass ratio of Pt/C and PTFE was 9:1. Subsequently, the cathode catalyst ink was sprayed directly onto the anion exchange membrane (A201,

28 μm, Tokuyama) with loadings of 1 mg_{Ag} cm^{-2}, and the anode catalyst was sprayed onto the carbon cloth (PTFE-treated, Fuel Cell Store) with loadings of 1.0 mg_{Pt} cm^{-2}. The final MEA was fabricated by mechanically sandwiching the cathode gas diffusion layer (SGL Carbon 25CC), the anion exchange membrane with cathode catalyst and the carbon cloth with anode catalyst. After fabrication, the MEA was mounted in the fuel cell hardware, to which high purity glycerol (99.8 wt%) and 100% humidified O_2 gas were supplied. A crude glycerol (88 wt%, directly obtained from soybean biodiesel production) was also directly used as anode fuel. The MEA was activated at 0.1 V until the current density got stable, and after that the polarization (*I*–*V*) curve was collected.

2.4. Electrochemical impedance spectroscopy (EIS) measurement

To measure the electrochemical behavior of MEAs with different sizes of Ag catalysts, the electrochemical impedance spectroscopy (EIS) was employed. A small AC signal was generated from the frequency analyzer and then applied to an electronic load to manipulate the DC load current. The current and voltage provided a connection between the electronic load and the fuel cell in order to monitor the current and voltage responses. Those AC voltage and current outputs from fuel cell were analyzed by the frequency response analyzer (880 impedance analyzer, Scribner-Associates, USA). The scheme of EIS set-up is illustrated in Fig. 1. In the test, the frequency of AC signal was varied from 10 mHz to 10 kHz, with amplitude of 5% DC current.

3. Results and discussion

The crystalline structure of two different particle sizes Ag/C catalysts (Ag/C-nanocapsule and Ag/C-commercial) was investigated by X-ray diffraction (XRD), as shown in Fig. 2. All of these diffraction patterns exhibit the characteristic peaks of the planes (111), (200), (220), (311) and (222) at 2θ angles of 39°, 44°, 65°, 77° and 83°, respectively. These numbers are assigned to the face centered cubic (fcc) crystalline structure of Ag (JCPDS card, 04-0783). It also indicates that Ag is in metallic state, because no characteristic peaks of silver oxide were found in their XRD patterns. The Debye–Sherrer equation (Equation (1)) was used to estimate the average crystal grain size, where τ is the mean size of the ordered (crystalline) domains, λ_{k_α} is the X-ray wavelength (1.5406 Å), β is the line broadening at half the maximum intensity (FWHM) in radians, θ is the Bragg angle and *K* is the shape factor

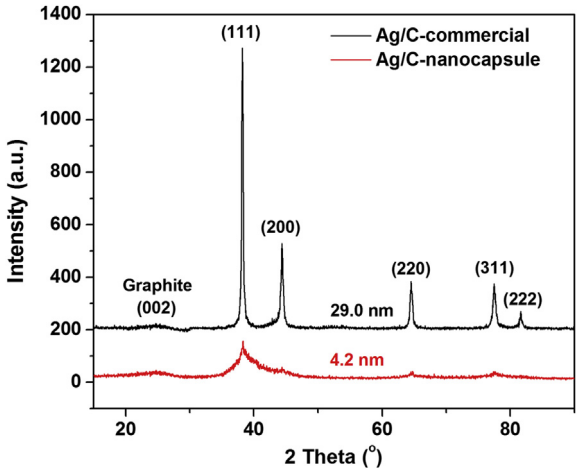

Fig. 2. XRD patterns of Ag/C-nanocapsule and Ag/C-commercial catalysts.

[30,31] (typical *K* value of 0.9 is used in here). From the calculation based on (220) peak, the particle sizes of Ag/C-nanocapsule and Ag/C-commercial are 4.2 nm and 29.0 nm, respectively.

$$\tau = \frac{K\lambda_{k_\alpha}}{B\cos\theta} \quad (1)$$

The morphology of as-synthesized catalysts was characterized by TEM. Images of Ag/C-nanocapsule and Ag/C-commercial catalysts are shown in Fig. 3(a) and (c). It is easy to note that the Ag particles are well dispersed on the surface of carbon black in the Ag/C-nanocapsule, and the particle size of Ag/C-nanocapsule is much smaller than that of Ag/C-commercial. The Ag/C-commercial is not only poor dispersed but also has a larger particle size. The corresponding particle size histograms evaluated from 100 random particles in an arbitrarily chosen area are shown in Fig. 3(b) and (d). The mean particle size of Ag/C-nanocapsule catalyst and commercial Ag nanoparticles are 5.4 nm and 27.4 nm, respectively, which agrees well with XRD results.

The polarization (*I*–*V*) and current density-power density curves of glycerol–O_2 AEM-DGFC are shown in Fig. 4(a). The cell operating temperature was set at 80 °C in order to facilitate the reaction kinetics and fuel diffusion [32]. From the *I*–*V* curve, it is observed that the open circuit voltages of the fuel cells with different cathode catalysts are 0.73 V (Ag/C-nanocapsule) and 0.68 V (Ag/C-

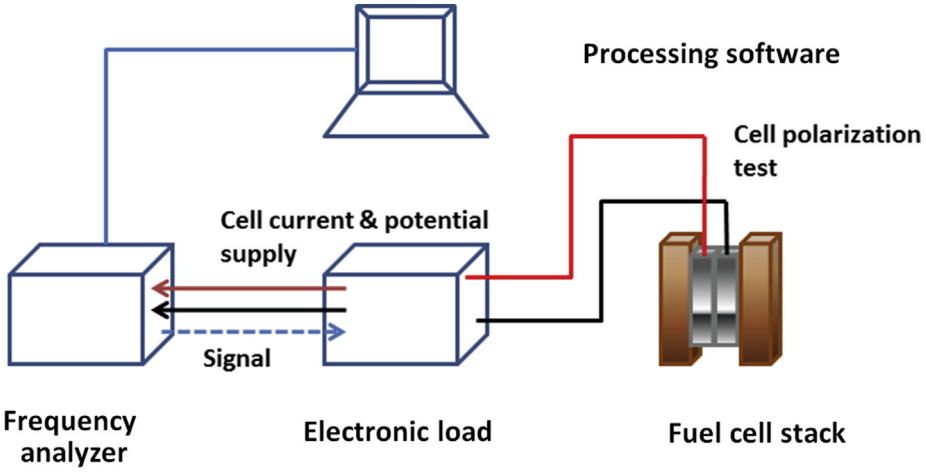

Fig. 1. Schematic illustration of electrochemical impedance spectroscopy (EIS) test equipment set-up.

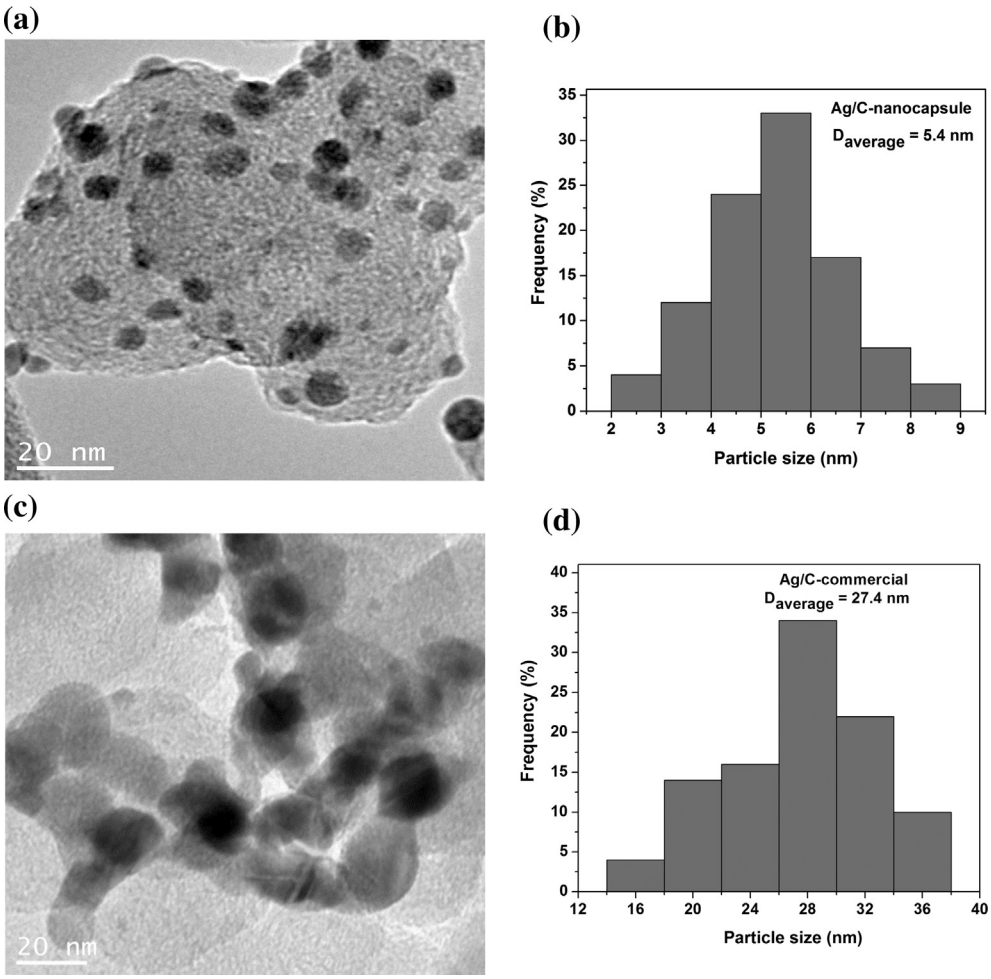

Fig. 3. TEM image and particle size histogram of Ag/C-nanocapsule (a, b) and Ag/C-commercial (c, d) catalysts.

commercial), respectively. Due to higher reaction rates and better oxygen diffusion, the peak power density of 86 mW cm^{-2} is achieved at the Ag/C-nanocapsule cathode-based AEMFC. By using the Ag/C-commercial as the cathode catalyst, the peak power density of AEMFC is only 45 mW cm^{-2}. Based on the analysis of the *I*–*V* curve, the fuel cell with Ag/C-nanocapsule cathode has over-performed the one with Ag/C-commercial cathode in both the kinetic dominated regime (current density is <50 mA cm^{-2}) and the ohmic resistance controlled regime (>50 mA cm^{-2}), which implies that higher activity and less performance loss due to the resistance to ionic current [33] were achieved on the Ag/C-nanocapsule catalyst. There's no obvious transport controlled regime on the *I*–*V* curve, and the possible reason is that both fuel cells cannot reach a very high current density (i.e. > 600 mA cm^{-2}). The better ORR activity on Ag/C-nanocapsule can be attributed to its smaller particle size [34,35]and uniform particle distributions [17,18]. It has been proven in a three-electrode system that through both the direct and indirect ORR pathways, the oxygen goes through the 4 steps, including O_2 adsorption, O–O bond breakage, and desorption of products, to complete the ORR [10,36]. The Ag/C with a smaller size has a higher surface area, thus leading to more catalytically active sites exposed, which can facilitate the oxygen reduction. Our fuel cell test confirms that this will facilitate ORR kinetics on Ag in single AEMFC. In addition, the results also show the particle size effect on ohmic loss in the fuel cell operation: the performance of fuel cell with the smaller cathode catalyst particle size dropped slowly during the test, which implies that using small size cathode catalyst can lead to less ohmic loss.

To further investigate the cathode and anode behaviors, a constant (cell) voltage test was conducted in order to get cathode and anode polarization curves. In this test, the anode and cathode overvoltage at constant fuel cell operation voltage of 0.5 V (near the OCV), 0.3 V (near the peak power density) and 0.1 V (near the limiting current) were measured. The test was performed at the setting potential, by looping 55 ml of 1.0 M glycerol + 2.0 M KOH from the anode fuel vessel into the anode plate channel, with the same cathode O_2 flow rate under 30 psi back pressure for 0.5 h. The anode potential was measured using an electronic load during the test: a Hg/HgO (1.0 M KOH) reference electrode was dipped into the anode fuel vessel, the electronic load was connected between the reference electrode and the fuel cell anode to make a closed loop. The potential could be read from the load, and this obtained potential value can be converted to a reversible hydrogen electrode (RHE) by $V_{\text{vs. RHE}} = V_{\text{measured vs. Hg/HgO/1.0 M KOH}} + 0.098 + 0.059 \times$ (pH of electrolyte solution). The cathode potential can be calculated using the equation below:

$$E_{\text{cathode}} = E_{\text{apply}} + E_{\text{anode}} + E_{\text{resistance}} \quad (2)$$

Where E_{cathode} is the cathode potential (vs. RHE), E_{apply} is the constant voltage applied on the test, E_{anode} is the measured anode potential and $E_{\text{resistance}}$ is the ohmic lost during the test, which can be calculated from measured average current density multiplied by fuel cell internal resistance (directly tested by the Scribner fuel cell stand). The *I*–*V* curves of cathode and anode are shown in Fig. 4(b).

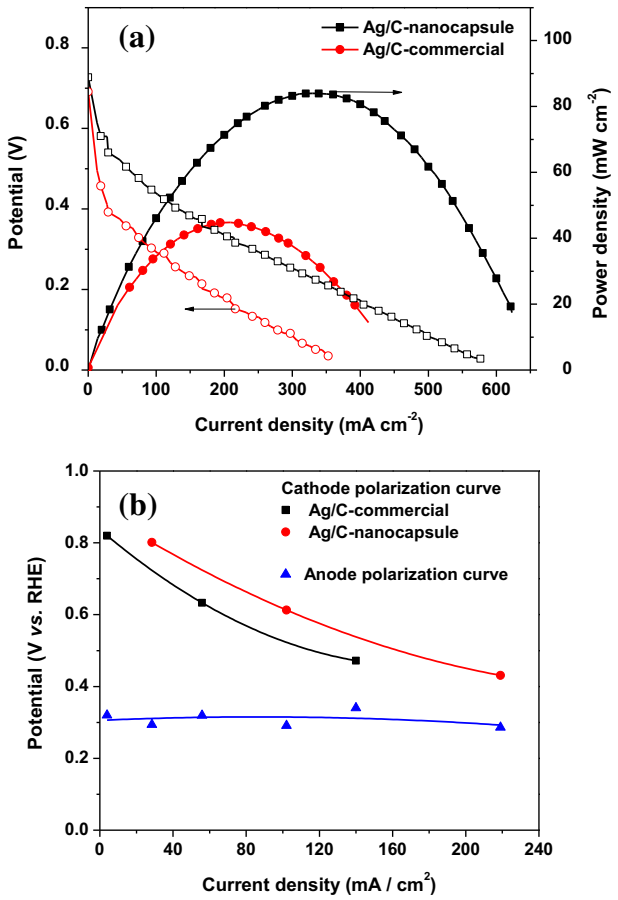

Fig. 4. (a) Polarization and power density of AEM-DGFC operating at 80 °C. Anode: Pt/C (40 wt% metal loading) 1.0 mg_{Pt} cm^{-2}; cathode: Ag/C-nanocapsule (40 wt% metal loading) or Ag/C-commercial (40 wt%) 1.0 mg_{Ag} cm^{-2}; 2.0 M KOH + 1.0 M glycerol; O_2: 0.4 L min^{-1}, 30 psi; (b) Separated polarization curves of anode (Pt/C) and cathode (Ag/C-nanocapsule and Ag/C-commercial) in fuel cell.

At the anode, all of the fuel cells (with different cathode catalysts) share a same trend, which can be fitted into a single curve, suggesting the polarization properties of both anodes are similar, and the electro-oxidation of glycerol under tested conditions is a fast process (compared with the sluggish ORR at the cathode). However, at the cathode, the cells show a different *I*–*V* trend. Because of the higher ORR activity on Ag/C-nanocapsule, the polarization on Ag/C-nanocapsule cathode is higher than that on Ag/C-commercial. In addition, the AEMFC with the Ag/C-nanocapsule catalyst can reach a higher limiting current density. These results confirm that the Ag/C-nanocapsule with small, uniformly dispersed nanoparticles is a better cathode catalyst compared to the commercial Ag/C with larger particle size.

It is very interesting to study crude glycerol as a fuel for the AEM-DGFC. The components of crude glycerol include 88 wt% of glycerol, 5.42 wt% of matter organic non glycerol, 4.16 wt% of moisture, 2.37 wt% of ash and 628 ppm of methanol. The fuel was used without any further treatment. Again, the fuel cell with Ag/C-nanocapsule cathode catalyst demonstrated a superior performance. The peak power density under the same operation conditions (same to the high purity glycerol AEMFC, Fig. 4) are 66 mW cm^{-2} and 38 mW cm^{-2} for Ag/C-nanocapsule and Ag/C-commercial catalysts, respectively, as shown in Fig. 5. By keeping the other test conditions identical, the catalyst particle size is still the dominant factor in governing the crude glycerol AEM-DGFC performance. Although the crude glycerol fuel cell performance (66 mW cm^{-2}) is lower than that of the high purity counterpart (86 mW cm^{-2}), it is still acceptable. The performance of these fuel cells (in terms of power density) is higher than that of glycerol–O_2 biofuel cell in magnitude orders [37,38]. This result demonstrates great potential of direct use of industrial-grade crude glycerol to generate electricity. However, the catalyst stability and operation stability associated with direct crude glycerol fuel cells should be investigated [33], and they are still underway in our lab.

The electrochemical impedance spectroscopy (EIS), which is also known as AC impendency technique, is capable of distinguishing the influences (voltage drop caused by charger transfer, membrane or mass transfer resistance) of the different processes (kinetic, ohmic or mass transport dominated) in the whole electronic system [39,40]. Herein, EIS is used to investigate the causes of the performance differences between the two fuel cells with different silver cathode catalysts. The resistance in high frequency regions could be attributed to the combined behavior of internal ohmic resistance and contact capacitance, the intercept of real component in *x*-axis is the reflection of the sum up of contact resistance and ohmic resistance (from cell components such as membrane and catalyst layer and the contact between each of them); the resistance in low frequency is charge transfer issue dominated, and the arc diameter in that location is inversely proportional to the ORR rate [41].

In our test, Nyquist diagrams obtained from the two fuel cells are shown in Fig. 6. In the spectra, although not that clear (due to the two arcs overlapping), one high frequency arc and one low frequency arc can still be observed. In the high frequency arc, the semicircle of Ag/C-nanocapsule is obviously smaller, which proves the fast kinetic process of ORR obtained on this catalyst. The higher surface area and more exposed catalytically active sites will definitely endow Ag/C-nanocapsule with higher ORR rate. Those results are in consistence with the *I*–*V* curves and the electrode polarization curves. In the high frequency regime, the spectrum of fuel cells using Ag/C-nanocapsule catalyst has relatively smaller intercept in real axis (z_{Re}) than that of Ag/C-commercial, which means the cell has low contact and ohmic resistances. Since there's no difference in the MEA and cell assembly between the two cells, the lower resistance of Ag/C-nanocapsule cell can be attributed to the catalyst layer. In the Ag/C-nanocapsule coated layer, small catalyst particle size can allow sufficient humidifying water to be held in the

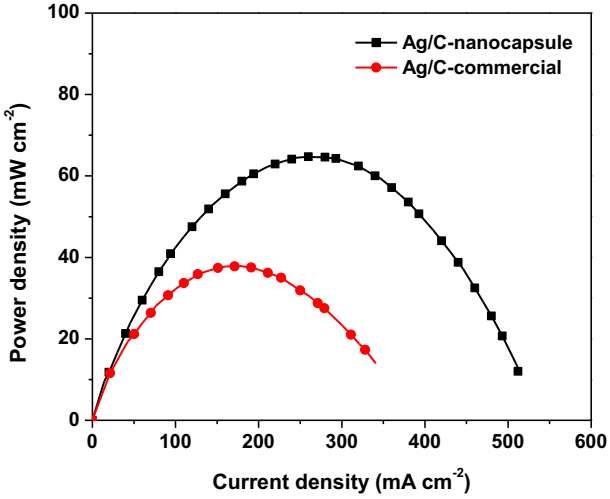

Fig. 5. Current density-power density curves of the AEM-DGFC operating at 80 °C. Anode: Pt/C (40 wt% metal loading) 1.0 mg_{Pt} cm^{-2}; cathode: Ag/C-nanocapsule (40 wt % metal loading) or Ag/C-commercial (40 wt%) 1.0 mg_{Ag} cm^{-2}; 2.0 M KOH + 1.0 M crude glycerol (88 wt%); O_2: 0.4 L min^{-1}, 30 psi.

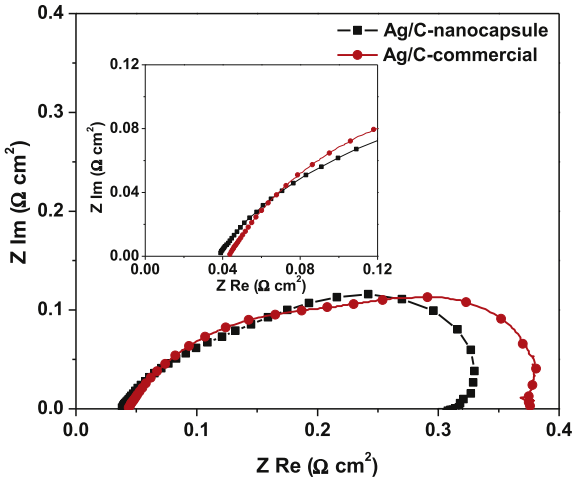

Fig. 6. EIS plots measured with the fuel cells using different particle size Ag/C cathode catalysts.

electrode, and the uniform particle distribution can prevent the agglomeration effect, which may lead to the boundary resistance increasing. Furthermore, the small particle and uniform distribution can decrease the migration path of ions, which can further reduce the distributed resistance. The high frequency EIS results provide the information that in the real fuel cell operation, the smaller cathode catalyst particle size will not only facilitate the ORR kinetics, but also reduce the performance loss that is due to the ohmic and contact resistances.

4. Conclusions

A solution phase-based nanocapsule method was developed to prepare the Ag/C-nanocapsule catalyst. The XRD and TEM characterizations reveal that Ag nanoparticles prepared by the nanocapsule approach have a small diameter of around 5.4 nm and narrow size distribution of 2–9 nm. To serve as control sample, the commercial Ag-NPs with a size of distribution 20–40 nm were deposited on carbon support using the impregnation method. Results of glycerol–O_2 anion exchange membrane fuel cells (AEM-DGFC) with Ag/C-nanocapsule and Ag/C-commercial cathode catalysts show that the fuel cell with smaller Ag particles has a higher ORR activity: the peak power density of 86 mW cm^{-2} was achieved on Ag/C-nanocapsule at 80 °C. In the constant voltage tests, with the same anode behavior, the AEMFC with the Ag/C-nanocapsule cathode can reach a higher current density and maintain less cathode overvoltage, as compared with the one with the Ag/C-commercial cathode. In the impedance test, the Ag/C-nanocapsule cathode-fuel cell shows a smaller arc and a smaller intercept in the real axis, which indicates a smaller kinetics resistance and a smaller contact/ohmic resistance, respectively. A crude glycerol was also served as fuel, and the AEMFC shows a promising performance of 66 mW cm^{-2}.

Acknowledgments

We acknowledge the US National Science Foundation (CBET-1032547, CBET1235982). Acknowledgment is also made to the Donors of the American Chemical Society Petroleum Research Fund for partial support of this research. W. Li thanks the support from Michigan Tech Research Excellence Fund – Research Seeds (REF-RS) grant E49290. Z. Wang thanks the Gray&Anderson Scholarship.

References

[1] I.S.A.I.C. EG&G Services. Parsons. Fuel cell handbook. 5th ed. Van Nostrand Reinhold; 2000.
[2] Antolini E, Gonzalez ER. Alkaline direct alcohol fuel cells. J Power Sources 2010;195:3431–50.
[3] Varcoe JR, Slade RCT. Prospects for alkaline anion-exchange membranes in low temperature fuel cells. Fuel Cells 2005;5:187–200.
[4] Yang C-C, Chiu S-J, Chien W-C. Development of alkaline direct methanol fuel cells based on crosslinked PVA polymer membranes. J Power Sources 2006;162:21–9.
[5] Matsuoka K, Iriyama Y, Abe T, Matsuoka M, Ogumi Z. Alkaline direct alcohol fuel cells using an anion exchange membrane. J Power Sources 2005;150:27–31.
[6] Coutanceau C, Demarconnay L, Lamy C, Léger JM. Development of electrocatalysts for solid alkaline fuel cell (SAFC). J Power Sources 2006;156:14–9.
[7] Spendelow JS, Wieckowski A. Electrocatalysis of oxygen reduction and small alcohol oxidation in alkaline media. Phys Chem Chem Phys 2007;9:2654–75.
[8] Kostowskyj MA, Kirk DW, Thorpe SJ. Ag and Ag-Mn nanowire catalysts for alkaline fuel cells. Int J Hydrogen Energy 2010;35:5666–72.
[9] Meng H, Shen PK. Novel Pt-free catalyst for oxygen electroreduction. Electrochem Commun 2006;8:588–94.
[10] Chatenet M, Genies-Bultel L, Aurousseau M, Durand R, Andolfatto F. Oxygen reduction on silver catalysts in solutions containing various concentrations of sodium hydroxide - comparison with platinum. J Appl Electrochem 2002;32:1131–40.
[11] Furuya N, Aikawa H. Comparative study of oxygen cathodes loaded with Ag and Pt catalysts in chlor-alkali membrane cells. Electrochim Acta 2000;45:4251–6.
[12] Okajima K, Nabekura K, Kondoh T, Sudoh M. Degradation evaluation of gas-diffusion electrodes for oxygen-depolarization in chlor-alkali membrane cell. J Electrochem Soc 2005;152:D117–20.
[13] Chatenet M, Micoud F, Roche I, Chainet E, Vondrák J. Kinetics of sodium borohydride direct oxidation and oxygen reduction in sodium hydroxide electrolyte: part II. O_2 reduction. Electrochim Acta 2006;51:5452–8.
[14] Blizanac BB, Ross PN, Markovic NM. Oxygen electroreduction on Ag(111): the pH effect. Electrochim Acta 2007;52:2264–71.
[15] Lima FHB, de Castro JFR, Ticianelli EA. Silver-cobalt bimetallic particles for oxygen reduction in alkaline media. J Power Sources 2006;161:806–12.
[16] Meng H, Wu M, Hu XX, Nie M, Wei ZD, Shen PK. Selective cathode catalysts for mixed-reactant alkaline alcohol fuel cells. Fuel Cells 2006;6:447–50.
[17] Varcoe JR, Slade RCT, Wright GL, Chen Y. Steady-state dc and impedance investigations of H_2/O_2 alkaline membrane fuel cells with commercial Pt/C, Ag/C, and Au/C cathodes. The J Phys Chem B 2006;110:21041–9.
[18] Park J-S, Park S-H, Yim S-D, Yoon Y-G, Lee W-Y, Kim C-S. Performance of solid alkaline fuel cells employing anion-exchange membranes. J Power Sources 2008;178:620–6.
[19] Maheswari S, Sridhar P, Pitchumani S. Carbon-supported silver as cathode electrocatalyst for alkaline polymer electrolyte membrane fuel cells. Electrocatalysis 2012;3:13–21.
[20] Avramov-Ivic M, Léger JM, Beden B, Hahn F, Lamy C. Adsorption of glycerol on platinum in alkaline medium: effect of the electrode structure. J Electroanal Chem 1993;351:285–97.
[21] Matsushita K, Yamashita T, Aoki N, Toyama H, Adachi O. Electron transfer from quinohemoprotein alcohol dehydrogenase to blue copper protein azurin in the alcohol oxidase respiratory chain of Pseudomonas putida HK5. Biochemistry 1999;38:6111–8.
[22] Bianchini C, Shen PK. Palladium-based electrocatalysts for alcohol oxidation in half cells and in direct alcohol fuel cells. Chem Rev 2009;109:4183–206.
[23] Zhang Z, Xin L, Li W. Supported gold nanoparticles as anode catalyst for anion-exchange membrane-direct glycerol fuel cell (AEM-DGFC). Int J Hydrogen Energy 2012;37:9393–401.
[24] Bambagioni V, Bianchini C, Marchionni A, Filippi J, Vizza F, Teddy J, et al. Pd and Pt–Ru anode electrocatalysts supported on multi-walled carbon nanotubes and their use in passive and active direct alcohol fuel cells with an anion-exchange membrane (alcohol = methanol, ethanol, glycerol). J Power Sources 2009;190:241–51.
[25] Xuan J, Leung MKH, Leung DYC, Ni M. A review of biomass-derived fuel processors for fuel cell systems. Renew Sust Energ Rev 2009;13:1301–13.
[26] Li W, Liang C, Zhou W, Qiu J, Zhou, Sun G, et al. Preparation and characterization of multiwalled carbon nanotube-supported platinum for cathode catalysts of direct methanol fuel cells. J Phys Chem B 2003;107:6292–9.
[27] Zhang Z, Xin L, Sun K, Li W. Pd–Ni electrocatalysts for efficient ethanol oxidation reaction in alkaline electrolyte. Int J Hydrogen Energy 2011;36:12686–97.
[28] Zhang Z, More KL, Sun K, Wu Z, Li W. Preparation and characterization of PdFe nanoleaves as electrocatalysts for oxygen reduction reaction. Chem Mater 2011;23:1570–7.
[29] Hacker V, Wallnofer E, Baumgartner W, Schaffer T, Besenhard JO, Schrottner H, et al. Carbon nanofiber-based active layers for fuel cell cathodes - preparation and characterization. Electrochem Commun 2005;7:377–82.
[30] Cullity BD, Stock SR. Elements of X-ray diffraction. 3rd ed. Prentice-Hall Inc.; 2001.
[31] Jenkins R, Snyder RL. Introduction to X-ray powder diffractometry. John Wiley & Sons Inc.; 1996.

[32] Zhang Z, Xin L, Li W. Electrocatalytic oxidation of glycerol on Pt/C in anion-exchange membrane fuel cell: cogeneration of electricity and valuable chemicals. Appl Catal B 2012;119–120:40–8.
[33] Li XG, Popov BN, Kawahara T, Yanagi H. Non-precious metal catalysts synthesized from precursors of carbon, nitrogen, and transition metal for oxygen reduction in alkaline fuel cells. J Power Sources 2011;196:1717–22.
[34] Chang Y-M, Wu P-W, Lin Y-M, Lin P, Chang Y-F, Liang R-M. Controlled synthesis of silver particles supported on carbon nanocapsules as electrocatalysts for oxygen reduction reaction in alkaline electrolyte. ECS Trans 2008;13:55–9.
[35] Lee C-L, Chiou H-P, Syu C-M, Wu C-C. Silver triangular nanoplates as electrocatalyst for oxygen reduction reaction. Electrochem Commun 2010;12:1609–13.
[36] Wagner N, Schulze M, Gülzow E. Long term investigations of silver cathodes for alkaline fuel cells. J Power Sources 2004;127:264–72.
[37] Arechederra RL, Treu BL, Minteer SD. Development of glycerol/O_2 biofuel cell. J Power Sources 2007;173:156–61.
[38] Arechederra RL, Minteer SD. Complete oxidation of glycerol in an enzymatic biofuel cell. Fuel Cells 2009;9:63–9.
[39] Mueller JT, Urban PM. Characterization of direct methanol fuel cells by ac impedance spectroscopy. J Power Sources 1998;75:139–43.
[40] Yuan X, Wang H, Sun JC, Zhang J. AC impedance technique in PEM fuel cell diagnosis—a review. Int J Hydrogen Energy 2007;32:4365–80.
[41] Liu F, Yi B, Xing D, Yu J, Hou Z, Fu Y. Development of novel self-humidifying composite membranes for fuel cells. J Power Sources 2003;124:81–9.